frontiers | Frontiers in Earth Science

TYPE Original Research
PUBLISHED 12 December 2024
DOI 10.3389/feart.2024.1517953

OPEN ACCESS

EDITED BY
Huaming An,
Kunming University of Science and Technology, China

REVIEWED BY
Antonio Giovanni Iaccarino,
University of Naples Federico II, Italy
Jian Ji,
Hohai University, China

*CORRESPONDENCE
Hongyan Deng,
annedeng@swjtu.edu.cn

RECEIVED 27 October 2024
ACCEPTED 29 November 2024
PUBLISHED 12 December 2024

CITATION
Yu M and Deng H (2024) Analysis of long-term creep response characteristics of high rock slopes considering cumulative effects of earthquakes.
Front. Earth Sci. 12:1517953.
doi: 10.3389/feart.2024.1517953

Analysis of long-term creep response characteristics of high rock slopes considering cumulative effects of earthquakes

Meilin Yu and Hongyan Deng*

School of Civil Engineering, Southwest Jiaotong University, Chengdu, China

In mountain-gorge areas, the rock creep is the critical process for high rock slopes failure. During long-term creep, slopes might encounter earthquakes and form further creep after earthquakes, which can easily lead to the slope failure. Based on a high rock slope in the Nujiang River Basin, deformation and dynamic response characteristics are analyzed by FLAC3D software, considering combined effects of multiple earthquakes and long-term creep. Results show that when the amplitude increases, the shear strength of the slope decreases and the risk of instability increases under combined actions of creep and earthquakes. Earthquakes promote the development of creep and induce the accumulation of damage on the slope surface and in the slope. The ground motion response on the slope surface is stronger than that in the slope, with the peak occurring at the top of the slope. Earthquakes have a greater impact on the middle and top of the slope surface, where cumulative damage and crack development begin. Vertical ground motion has a great effect on the dynamic response. The slope resonance leads to a larger PGA amplification factor in the vertical direction than that in the horizontal direction. Nonlinear and damping characteristics of the slope and the frequency of seismic waves cause the PGA amplification factor to decrease with increasing amplitudes. This study could promote the development of high rock slope failure mechanism and provide references for the prevention of landslides in the Nujiang River Basin.

KEYWORDS

long-term creep response, multiple earthquakes, high rock slope, cumulative effect, deformation characteristic, dynamic response

1 Introduction

In mountain-gorge areas, the modern tectogenesis is intense and the landscapes have been eroded violently by rivers. Influenced by the special seismic geological environment and complex mechanical conditions, the rock mass of the high rock slope has undergone intense supergene transformation and formed a large number of fractured rocks which contain more structure planes and joint cracks. In addition to the external force, the rock mass is more prone to creep. The creep of high rock slopes is a general concept. We need to take into account not only the creep properties of the rock material itself in a narrow sense, but also the influence of external factors on it, such as seismic effects.

Although the initial mechanical state of the slope is in equilibrium, the long-term self-weight and external force will make the distribution of stress field and mechanical parameters of the slope change continuously. Starting from the localized high stress level zone of the rock mass, after a long period of creep, the slope gradually develops into instability (Huang et al., 2021). When the shear failure occurs, the slope structure is unstable and sliding failure may bring huge impacts and disasters to people's life and property safety (Deng et al., 2023; Huang et al., 2023). After a period of creep, the slope in the seismic region is easy to undergo large deformation due to seismic action, which will lead to stress redistribution of the rock mass. The slope will undergo creep deformation different from that before the earthquake. The whole process of mechanical response from creep to earthquake and creep after earthquake is very complex (Wang et al., 2011). Then there's great theoretical value and practical research significance to carry out risk research work on such slopes.

At present, the numerical simulation method has proved to be an effective tool to simulate the creep process of high rock slopes. Many scholars deeply studied the creep characteristics of high rock slopes and developed diverse creep models (Zhou and Cheng, 2015; Zhang et al., 2019; Li A. R. et al., 2021; Li M. J. et al., 2021; Sun et al., 2023). Numerous studies focused on the creep acceleration stage of rocks of slopes and deeply probe into the nonlinear fluid mechanics. They proposed many nonlinear creep models which can better reflect the damage of rocks of slopes in the accelerated stage of creep (Jiang et al., 2019; Li et al., 2019; Zhen, 2021; Lei and Sornette, 2023; Bao et al., 2024). In terms of the effect of external forces on creep development, scholars explored the trend of long-term creep development of slopes considering rainfall, river cutting and excavation through practical slope cases (Luo et al., 2008; Vallet et al., 2016; Li M. J. et al., 2021; Bao et al., 2022; Jeng et al., 2022; Delchiaro et al., 2023; Dong et al., 2023; Paul et al., 2024). From the above, most of studies focused on the creation and selection of constitutive models. In terms of external forces, scholars focused on rainfall, river cutting, engineering activities. However, there are few numerical studies on the long-term creep response of high rock slope under earthquake action. This study will fill this gap.

Currently, worldwide scholars have conducted in-depth and detailed researches on the post-earthquake dynamic response of rock slopes and obtained rich research results. However, traditional studies on the seismic dynamic response of rock slopes only focused on the seismic effects in the horizontal direction and ignored those in the vertical direction (Yan et al., 2011; Sun et al., 2022). In fact, results of existing studies show that vertical seismic action has a great influence on the seismic response of rock slopes (Huang et al., 2010; Che et al., 2016; Chen et al., 2017b; Song et al., 2018; Fan et al., 2020; Tang et al., 2021). So both horizontal and vertical ground motions should be considered in the dynamic analysis of rock slopes. General research methods are mainly divided into the following categories: theoretical analysis, physical model test and numerical simulation, etc., (Dong et al., 2013; Chen et al., 2017a; Xu et al., 2017; Song et al., 2019). Theoretical analysis methods are mainly categorized into pseudo-dynamic method, pseudo-static method, Newmark sliding block method, Pareto optimality and so on (Deng et al., 2014; Büyük et al., 2020; Hu et al., 2023; Zhou et al., 2023; Hu et al., 2024; Ji et al., 2024). Physical modeling experiments are usually divided into shaking table tests and dynamic centrifuge model tests (Sun et al., 2017; Lian et al., 2023).

The numerical simulation method is widely used in the seismic analysis of rock slopes because of its advantages of not being restricted by site, repeatability, and solving the seismic problem of slope efficiently and quickly (Bowa et al., 2018; Yan et al., 2020; Antwi Buah et al., 2023; Xiong et al., 2023). The dynamic time-history analysis method is generally used in numerical simulation (Peng, 2017). Most researchers considered the single earthquake when they discussed the law of deformation and failure of rock slopes under earthquakes. Less attention has been paid to the effect of cumulative damage on the dynamic response of slopes under multiple earthquakes, which may lead to a significant decrease in slope stability. A few scholars made a preliminary exploration (Li, 2015; Liu et al., 2018; Yang Z. P. et al., 2018), which mainly focused on the study of the stability of rock slopes under frequent micro-earthquakes, but lacks the study of the response of rock slopes under multiple earthquakes with different intensities. There are relatively few related studies, which are mainly due to the limitation of shaking table test equipment and methods consuming a lot of time and cost. In this paper, FLAC3D (Itasca Consulting Group, 2020) is used to carry out the numerical simulation, which can help us comprehensively and efficiently predict the cumulative damage behaviors of slope rocks under multiple seismic actions.

In conclusion, the present research results can not reflect the dynamic response characteristics of high rock slopes under multiple earthquake actions, nor can they fully consider characteristics of the long-term creep response of high rock slopes under earthquake actions. Therefore, to research characteristics of the long-term creep response of high rock slopes considering the cumulative effect of bidirectional earthquakes, a slope in Nujiang River Basin in southwest China is taken as an example. Using FLAC3D finite element software, in the case of multiple actions of earthquakes with different peak accelerations and long-term creep at the same time, the process of experiencing multiple earthquakes during the 100-year creep process is simulated to analyze deformation characteristics and dynamic response laws of the high rock slope. This research could provide references for the prevention and treatment of geological disasters of similar slopes in the Nujiang River Basin of southwest China.

2 Study area

Nujiang River is one of the largest rivers in southwest China, originating from the Qinghai-Tibet Plateau and flowing through Yunnan and the Tibet region. The study area is located upstream of Nujiang River and flows through Basu County, Milin County in the Tibet. The geographical location of the study area is shown in Figure 1A. The slope is only 200 m away from Nujiang River (Figure 1B). The study area is located in a stretch of river with a deep valley and steep hills on both sides. The geological profile of the slope is shown in Figure 2A. The topography of the slope is narrow and long, sloping gradually from east to west. The slope angle is about 46°. The layer of the rock is inclined at a low angle along the direction of the river. The rock and soil mass of the slope presents a reverse dip structure. The stratigraphy that occurs from top to

bottom of the slope is fragmented and strongly weathered quartz schist, weakly weathered quartz schist, weakly weathered crushed granite, weakly weathered granite, and slightly weathered granite. The overlying bedrock is mainly fragmented and strongly weathered quartz schist, which is more seriously affected by weathering, and the fissure surface is rough and mostly gray-yellow. The thickness of the layer is generally about 10 m and the rock quality is softer, easily broken by hammering. Its compressive strength is lower than that of other rocks, with a depth of 373 m and a dip angle of 52°–67°.

The following data below are all from the National Earthquake Data Center (China Earthquake Networks Center, 2006). The study area is located at the junction of tectonic plates, surrounded by several active faults. The study area is located on the Bangonghu-Nujiang fault (yellow line in Figure 1A). Southern and western sides of the study area are in the Himalayan region, which is characterized by strong seismicity. The major faults affecting the Himalayan region are the Yarlung Zangbo River fault (light blue line in Figure 1A) and the southern Tibet detachment system fault (brown line in Figure 1A). As of 2020, a total of 1,402 earthquakes with magnitude (M) greater than 4.7 have been recorded, including 142 earthquakes of magnitude 6–6.9, 24 earthquakes of magnitude 7–7.9, and 9 earthquakes of magnitude greater than 8. The northern side of the study area is within the Qinghai-Tibet Plateau. The Ganzi-Yushu fault (green line in Figure 1A) has shown strong seismic activity recently which has a great impact on the region. As of 2020, a total of 510 earthquakes with magnitude (M) greater than 4.75 have occurred in this zone, including 63 earthquakes of magnitude 6–6.9, 7 earthquakes of magnitude 7–7.9, and 2 earthquakes of magnitude greater than 8. The most active fault of the eastern side of the study area is the Xianshuihe-Anninghe-Xiaojiang fault (purple line in Figure 1A). As of 2020, a total of 763 earthquakes of magnitude greater than 4.7 have been recorded, including 109 earthquakes of magnitude 6–6.9, 32 earthquakes of magnitude 7–7.9, and one earthquake of magnitude greater than 8. These fault zones entered a new period of activity after 1930. So the seismicity of the region in the next 100 years is considered at a relatively active level with the possibility of breeding and generating strong earthquakes.

Based on this geological background, the region has strong neotectonic movement and relatively fragile geological conditions. The seismic activity has become one of the important influences affecting the long-term creep of slopes in the upper part of Nujiang River Basin.

3 Computational model and method

3.1 Computational model

In this paper, the explicit finite difference software FLAC3D is used for the numerical simulation, which can efficiently and accurately simulate the static or dynamic response in geotechnical engineering. Due to the large workload of calculating the actual slope model, the generalized model is adopted for the study. According to the results of geological investigation, the real slope morphology is simulated by contour data, and then the geological profile (Figure 2A) is divided into five strata as a prototype. Among them, fragmented and strongly weathered quartz schist is a soft rock, which is formed in the tectonic fragmentation zone, and the thickness of the rock layer is 10 m. Other rocks are harder and have larger rock parameters. Dimensions and meshes of the simple model of the slope are shown in Figure 2B. The length of the model is about 962 m (X-axis direction), the height is about 753 m (Z-axis direction), the width is about 200 m (Y-axis direction), and the slope is about 46°. In order to facilitate the division of units, the three-dimensional model uses all hexahedral units, and the slope model has a total of 41,743 units and 39,583 nodes.

The mesh size has an impact on the accuracy of the dynamic computational analysis (Antwi Buah et al., 2023). The more the number of meshes is, the higher the computational accuracy is. However, overly dense meshes can also make the computation too slow. To ensure both computational accuracy and speed, it is necessary to adopt an appropriate mesh division. Lysmer pointed out (Lysmer and Kuhlemeyer, 1969) that in order to more accurately characterize the propagation of seismic waves in the numerical model, the model cell size needs to satisfy the following equations (Equations 1, 2):

$$\Delta l \le n\lambda \tag{1}$$

$$n = 0.100 \sim 0.125 \tag{2}$$

Where:

Δl—Maximum size of model unit;

λ—The shortest wavelength corresponding to the frequency components of the input wave in the seismic record.

Calculated from the above equation (Equations 1, 2), the shortest wavelength corresponding to the frequency components of the input wave in the seismic record is 127.75 m. The maximum grid size of the model unit is 12.775–15.969 m. Considering the balance between computational accuracy and time consumption, the maximum grid size of the model unit is set to 14 m.

3.2 Parameter and constitutive model

For simulation modeling, physical and mechanical parameters of rocks obtained through field investigation and indoor tests are shown in Table 1. For mechanical creep parameters of fragmented and strongly weathered quartz schist, Maxwell shear modulus is 1.15 GPa, Kelvin shear modulus is 0.98 GPa, Maxwell viscosity is 16,400 GPa s and Kelvin viscosity is 4,570 GPa s.

In the numerical model, the rocks can be divided into two categories. One is the hard rock that does not need creep calculation, and the other is the soft rock that needs creep calculation. The soft rock has low compressive strength, obvious rheological properties, and large creep deformation, which often causes slope instability and damage. It generally has transient elasticity, transient plasticity, viscoelasticity and viscoelasticity. Burgers-Mohr model (Itasca Consulting Group, 2020) built in FLAC3D can comprehensively describe the viscoelastic-plastic properties of the medium, and can describe the whole process of the rock creep curve, including the attenuation creep, the uniform creep stage and the accelerated creep stage. Several scholars have proved through

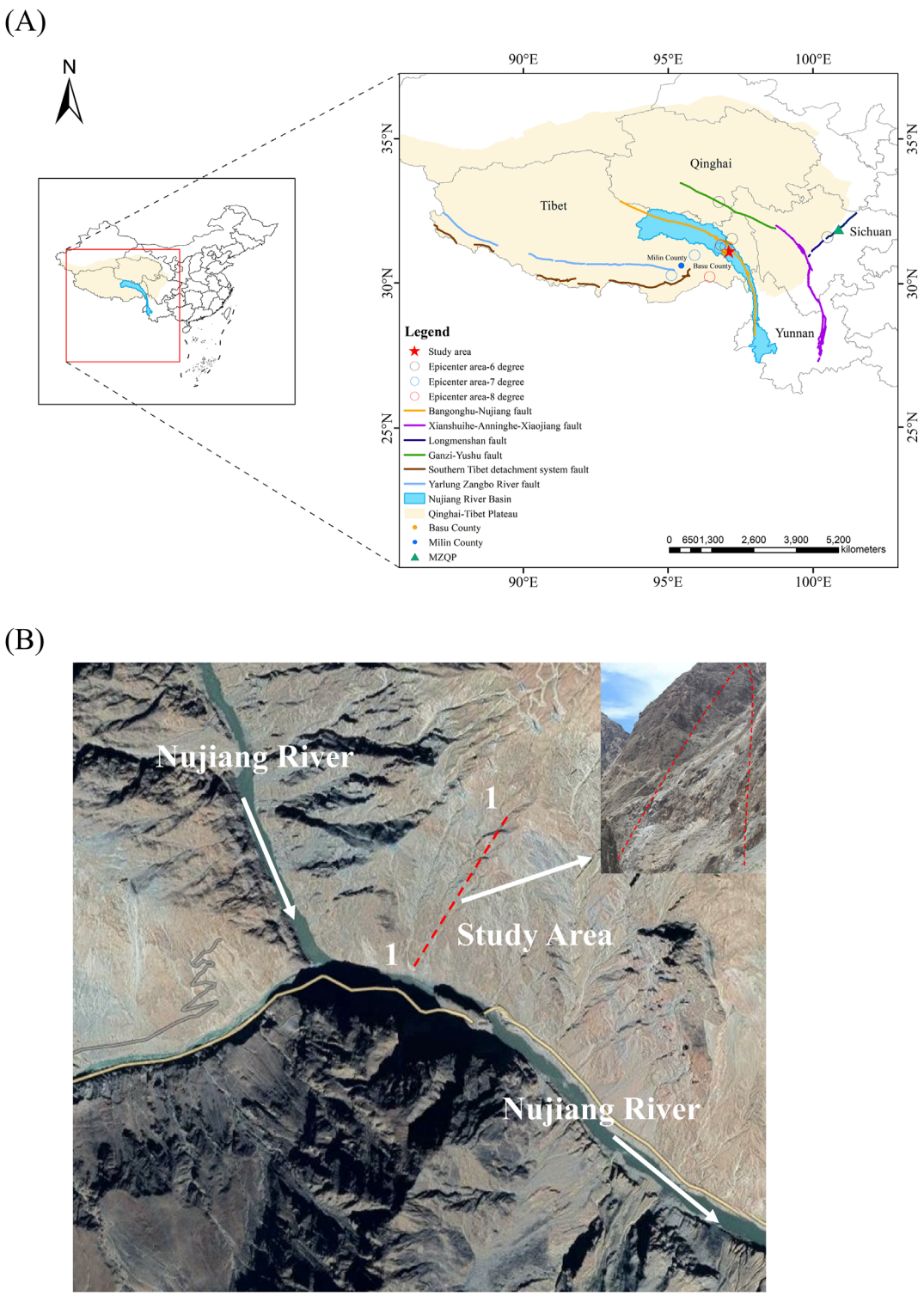

FIGURE 1
Location of the study area and the slope. **(A)** Geographical location of the study area. **(B)** Slope location.

researches that the Burgers-Mohr model can well describe the creep properties of soft rocks (Yuan et al., 2006; Guo et al., 2023; Chu et al., 2024). According to the above analysis, in the creep calculation, the fragmented and strongly weathered quartz schist (hereafter referred to as the cataclastic rock) has characteristics of rock body fragmentation and softer rock. The cataclastic rock is considered as a soft rock that will undergo creep and is simulated by the Burgers-Mohr model. Other rocks with larger rock parameters

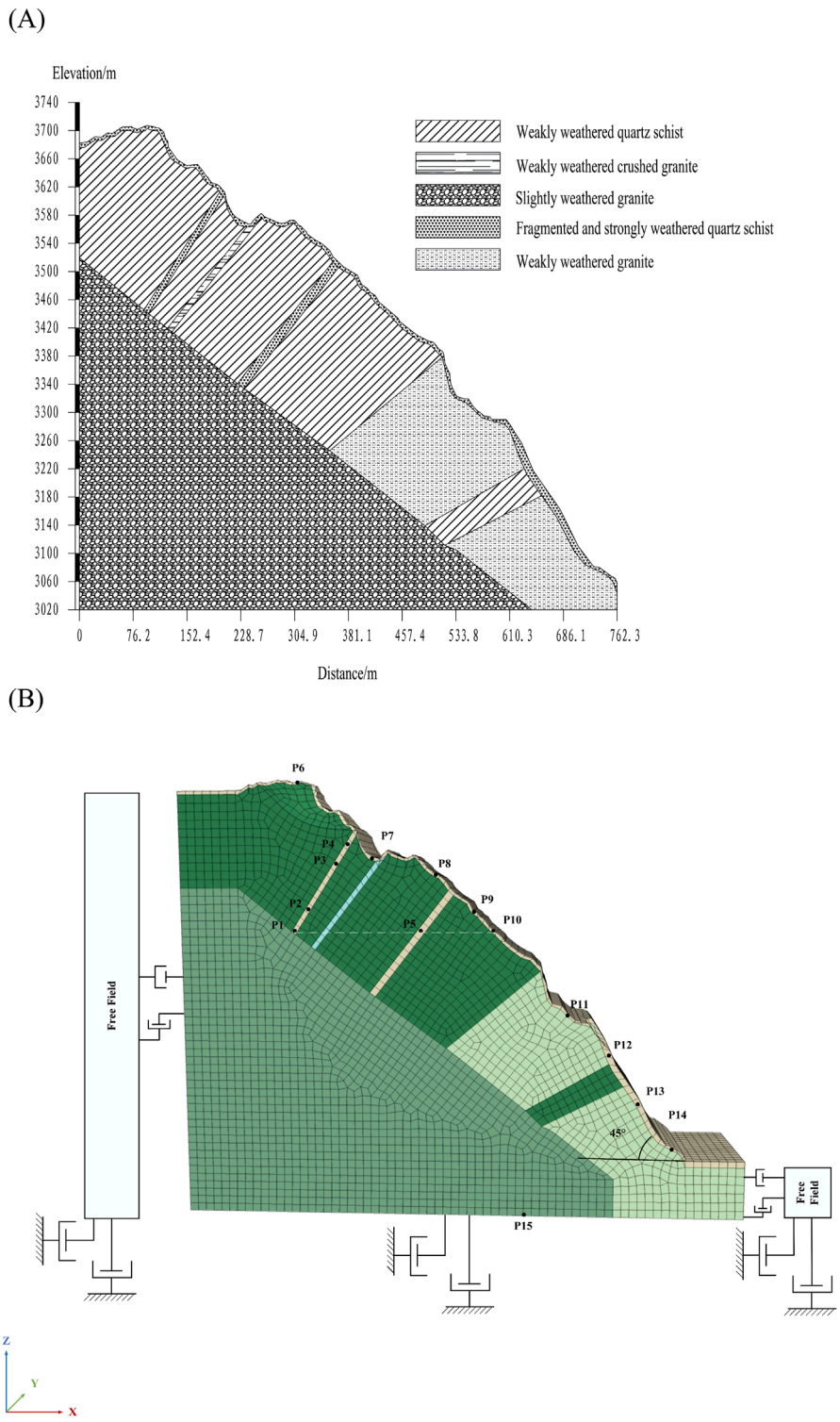

FIGURE 2
Numerical model. **(A)** 1-1 cross-sectional diagrams for modeling. **(B)** Dimensions, boundary conditions and the layout of monitoring points of the slope model.

are not considered to undergo creep, so they are simulated by the Mohr-Coulomb model (Itasca Consulting Group, 2020).

For the dynamic calculation, the Burgers-Mohr model is used in the form of viscoelastic increments and satisfies the following relationship (Equation 3). In the dynamic calculations, the creep calculation switch is off, which is equivalent to a creep time step of 0. The viscous progenitor in the Burgers-Mohr model does not effectively represent the time of the mechanical

TABLE 1 Physical and mechanical parameters of the rocks.

Category of rock	Volume weight γ/(kN·m^{-3})	Cohesion c/(MPa)	Frictional angle φ/(°)	Elasticity modulus E/(GPa)	Poisson ratio μ
Fragmented and strongly weathered quartz schist	25	0.4	32	2	0.32
Weakly weathered quartz schist	27.1	1.2	48	35	0.21
Weakly weathered granite	26	1.6	50	30	0.22
Weakly weathered crushed granite	25.5	0.6	37	15	0.25
Slightly weathered granite	26.4	1.8	52	40	0.20

behavior of the material, and the unit exhibits an elastoplastic stress-strain relationship, which behaves in the same way as an elastoplastic material.

$$\varepsilon = \frac{\sigma}{E_M} + \frac{\sigma}{\eta_M}t + \frac{\sigma}{E_K}\left(1 - e^{-\frac{E_K}{\eta_K}t}\right) + \varepsilon_p \tag{3}$$

Where:
ε—Total strain;
σ—Total stress;
ε_p—Plastic body strain;
E_M—Maxwell shear modulus;
E_K—Kelvin shear modulus;
η_K—Kelvin viscosity factor;
η_M—Maxwell coefficient of viscosity.
When $t = 0$, Equation 3 is converted to Equation 4:

$$\varepsilon = \frac{\sigma}{E_M} + \varepsilon_p \tag{4}$$

For the Mohr-Coulomb model, the strain increment is decomposed into an elastic part and a plastic part according to the elastoplastic theory, satisfying the following equation (Equation 5):

$$\varepsilon = \varepsilon_M + \varepsilon_P \tag{5}$$

Where:
ε_M—Elastic body strain
The expression based on Hooke's law is as follows (Equation 6):

$$\varepsilon_M = \frac{\sigma}{E_M} \tag{6}$$

Combining Equations 5, 6, the Mohr-Coulomb model satisfies the following relationship (Equation 7):

$$\varepsilon = \frac{\sigma}{E_M} + \varepsilon_p \tag{7}$$

Through Equations 4, 7, it can be seen that the Burgers-Mohr model exhibits the same properties as the Mohr-Coulomb model. Therefore, all rocks are assigned the Mohr-Coulomb model in the dynamic calculation. To further verify the reasonableness of the selection of the principal structure, FLAC3D software is used to conduct conventional triaxial compression tests of the rock, utilizing a single unit with a total of 8 nodes and 4 nodes on the fixed bottom surface, applying the same circumferential pressure in the X, Y and Z directions to the unit and axial pressure along the Z-axis direction. The Burgers-Mohr model and Mohr-Coulomb model are assigned respectively. Results show that the displacement is almost the same, which verifies the rationality of the selection of the constitutive model.

3.3 Boundary condition and layout of monitoring points

When seismic action is carried out, the static calculation is carried out first, and then the dynamic calculation is analyzed. For static calculation, the initial stress field generated by the self-weight of the rock mass is considered. The four sides in X direction and Y direction are normal constraints. The bottom is fixed constraints and the top of the slope is a free boundary. For dynamic calculation, the use of quiet boundary and free-field boundary can avoid the problem of wave reflection on the boundary. The research object is a rock slope. The bedrock modulus is large and the bottom is the rigid foundation. So the quiet boundary is used at the bottom. Four sides of the model in the X direction and Y direction use free-field boundaries, as shown in Figure 2B.

The layout of monitoring points for the slope model is shown in Figure 2B. Nine monitoring points at different elevations in the vertical direction of the slope surface (P6-P14), four monitoring points at different relative elevations in the vertical direction of the slope (P1-P4), and three monitoring points at the same elevation in the horizontal direction of the slope (P1, P5, P10) are selected.

3.4 Ground vibration synthesis and input

In order to try to ensure the accuracy of calculation results, Rayleigh damping is adopted. The critical damping ratio of

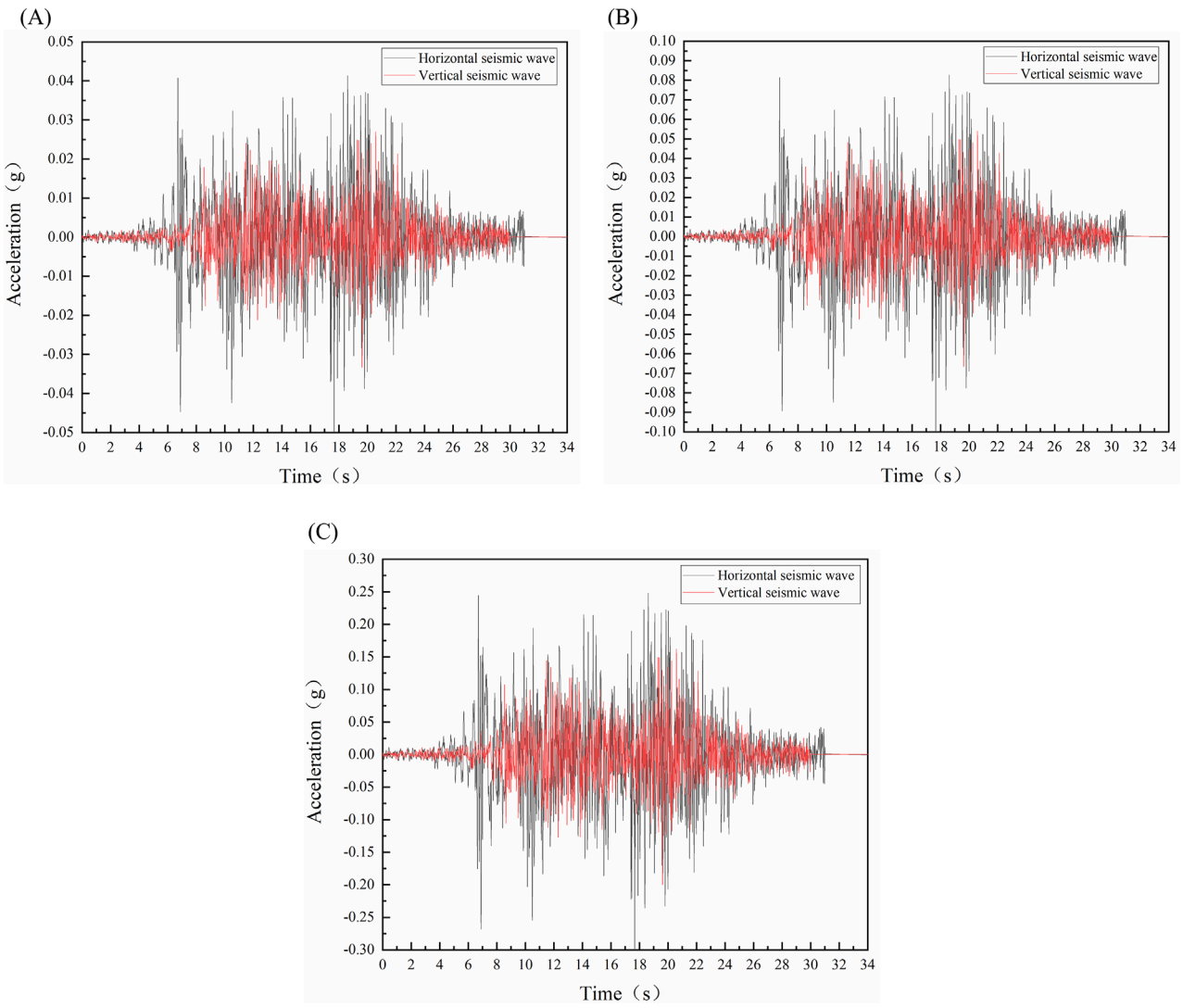

FIGURE 3
Acceleration time-range curves of input horizontal and vertical seismic wave. **(A)** Amplitude 0.05 g; **(B)** Amplitude 0.1 g; **(C)** Amplitude 0.3 g.

geotechnical materials is generally taken as 2%–5%. The minimum critical damping ratio is taken as 0.04. The center frequency is taken as the superposition of the input frequency and the system's self-oscillation frequency.

According to the seismic ground motion parameter zonation map of China (GB18306-2015) (China earthquake disaster prevention center, 2015), the site of the slope belongs to a Class II site. The seismic precautionary intensity is VII degree and the basic peak seismic horizontal acceleration is 0.1 g. The seismic precautionary intensity is the seismic intensity approved by the national authority as the basis for earthquake resistance in a region. On 12 May 2008, Wenchuan Ms8.0 earthquake occurred, with tens of thousands of aftershocks being generated against this tectonic background. Wenchuan earthquake was a large earthquake of the reverse dip-slip type that occurred in the continental interior. Its focal mechanism is dominated by the uplift and slip type. The earthquake source is planar, with a rupture zone nearly 300 km long. The earthquake focal depth reaches 12 km. The maximum displacement reaches 9 m and the seismic vibration response is extremely strong (Cai et al., 2011; Hu et al., 2012; Wen et al., 2014). Utilizing the seismic motion data provided by the China Earthquake Networks Center (Institute of Geophysics, 2004), the records from the MZQP station, which is in proximity to the primary seismic fault zone (the Longmenshan fault marked with deep blue line in Figure 1A), are selected to serve as the input for our analysis. This station boasts a rich and consistently recorded dataset. The coordinate of the MZQP station is (31.5°N, 104.1°E), as shown in Figure 1. The Wenchuan earthquake is one of the most complete sets of seismic earthquake data recorded in China to date. There is a certain similarity in the formation mechanism of the Longmenshan fault in the Wenchuan area and the Bangonghu-Nujiang fault in the study area. In order to be close to the actual situation, considering that the Wenchuan earthquake has a large impact on the area where the slope is located, the E-W direction component and the vertical component of the Wenchuan wave are selected as the inputs of the horizontal and vertical ground motion respectively, and the

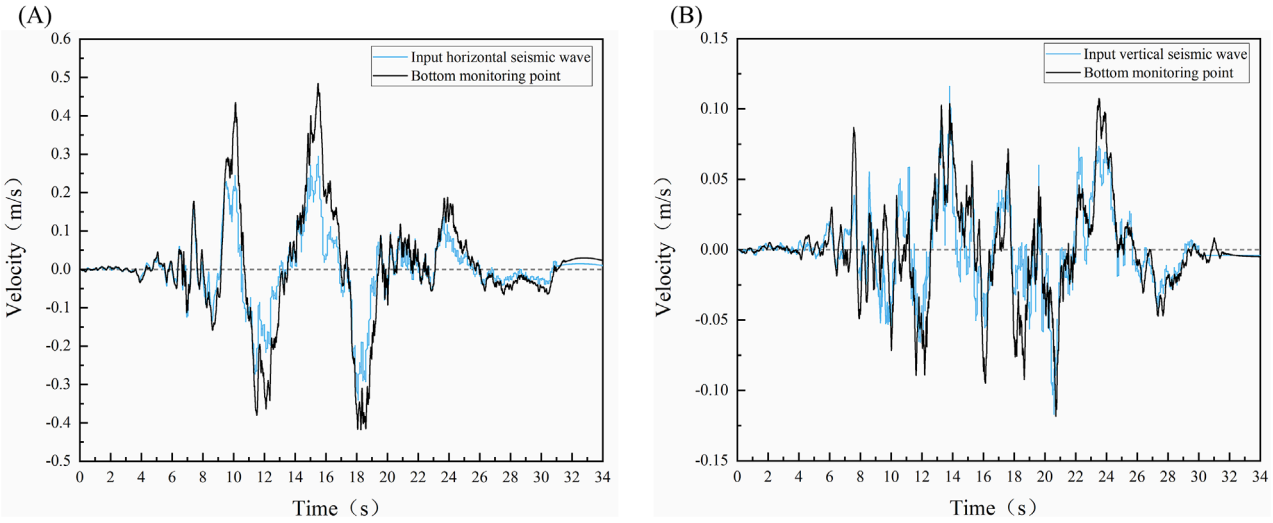

FIGURE 4
Comparison between the velocity time range of the point P15 and the input seismic wave. **(A)** Horizontal ground motion; **(B)** Vertical ground motion.

TABLE 2 Earthquakes have a greater impact on the area where the slope is located in the last 100 years.

Year	Magnitude	Epicenter area	Calculated intensity	Seismic precautionary intensity
1947	7.7	The southeast region of Lang County in Tibet	5.6	7
1950	8.6	Chayu and Medog in Tibet	7.5	8
1951	6	Chamdo in Tibet	5.2	6
1953	5.5	Basu in Tibet	7.2	8
1984	5.1	The southwest region of Markham in Tibet	5.9	7
1997	5.2	The southwest region of Zuo Gong in Tibet	5.3	6
2008	8	Wenchuan in Sichuan	4.9	6
2010	7.4	Yushu in Qinghai	5.3	6
2017	6.9	Milin in Tibet	5.5	7

area where the ground motion effect is most concentrated in the mainshock portion is intercepted. The simulation time is set to 34s, and Seismosignal (Seismosoft, 2021) is used for filtering and baseline correction.

When considering the input of seismic waves with different peak accelerations, the seismic waves are scaled proportionally to maintain the consistency of the seismic waves. Based on the code for seismic design of railway engineering (GB 50111–2006) (Ministry of Construction of the People's Republic of China, 2009), intensities of 6°, 7° and 8° are adopted to assess the long-term creep response of the slope under earthquakes with different peak accelerations. The corresponding peak accelerations (In the following text, it is referred to as amplitudes) of horizontal earthquakes are 0.05 g, 0.1 g and 0.3 g respectively. The peak acceleration of vertical ground motion is taken as a 2/3 value. The seismic acceleration time range converted to stress time range is loaded at the bottom of the slope and input vertically upward from the bottom boundary of the model. The horizontal and vertical acceleration time-range curves for different peak accelerations are shown in Figure 3.

The monitoring point P15 is set at the bottom of the model to verify whether the modeling and seismic wave input are correct or not, by comparing the velocity time range of the monitoring point at the bottom with the velocity time range of the input seismic wave. Taking the working condition of amplitude 0.05 g as an example (Figure 4), in the horizontal and vertical directions, the velocity time course monitored at the bottom point P15 and the velocity time course of the input seismic wave are basically the same, which indicates that the model is built correctly and the ground motion is input in the correct way.

TABLE 3 Seismic and creep modes of action for different amplitudes.

Order of action \ Amplitude	0.05 g	0.1 g	0.3 g
1	34s earthquake action	34s earthquake action	34s earthquake action
2	25-year creep effect	30-year creep effect	50-year creep effect
3	34s earthquake action	34s earthquake action	34s earthquake action
4	25-year creep effect	30-year creep effect	50-year creep effect
5	34s earthquake action	34s earthquake action	
6	25-year creep effect	40-year creep effect	
7	34s earthquake action		
8	25-year creep effect		

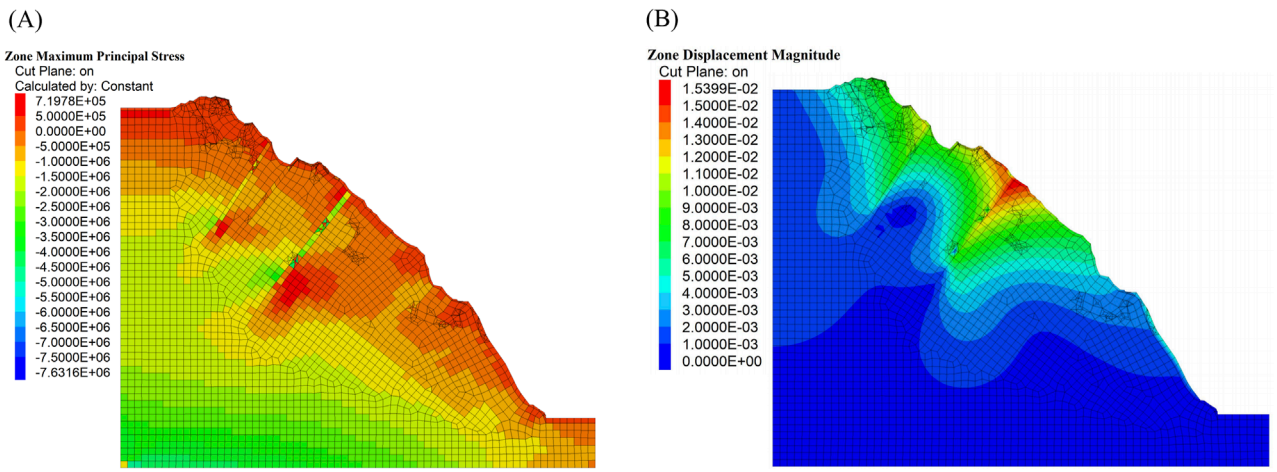

FIGURE 5
The contour of total displacement and maximum principal stress after 100-year creep of the slope without earthquake action: **(A)** Maximum principal stress (unit: Pa); **(B)** Total displacement (unit: m).

3.5 Design of computational scenarios

In this paper, different peak accelerations are used as the control factor to analyze the change rule of the dynamic response of the slope under the action of bidirectional ground motion. According to the data of the National Earthquake Data Center (China Earthquake Networks Center, 2006) and the geological exploration, we can count the earthquakes which have a great influence on the area where the slope is located in the past 100 years (Table 2). The calculated intensity is the intensity obtained through the attenuation relationship of the average axis of intensity in the western region of China, based on the impact of historical earthquakes on the study area (Yu, 2016). The seismic precautionary intensity is the earthquake intensity determined by the complexity of the site, the importance of the project, and the severity of the consequences caused by earthquakes. In order to determine the peak acceleration of horizontal ground motion corresponding to the seismic precautionary intensity which is generally an integer, the seismic precautionary intensity is generally the value obtained by rounding up after increasing the calculated intensity by one degree and then rounding to the nearest whole number.

A total of four earthquakes have affected the site in the area with an intensity of VI degrees, a total of three earthquakes have affected the site in the area with an intensity of VII degrees, and a total of two earthquakes have affected the site in the area with an intensity of VIII degrees. Therefore, three sets of working conditions are designed at amplitudes of 0.05 g, 0.1 g, and 0.3 g respectively. Seismic and creep modes of action for different amplitudes are shown in Table 3.

The calculation procedure is divided into the following steps:

(1) Firstly, an elastic constitutive model is assigned to rocks, the gravity load is applied to the model, and calculation is carried out until equilibrium in order to obtain the initial stress field of the

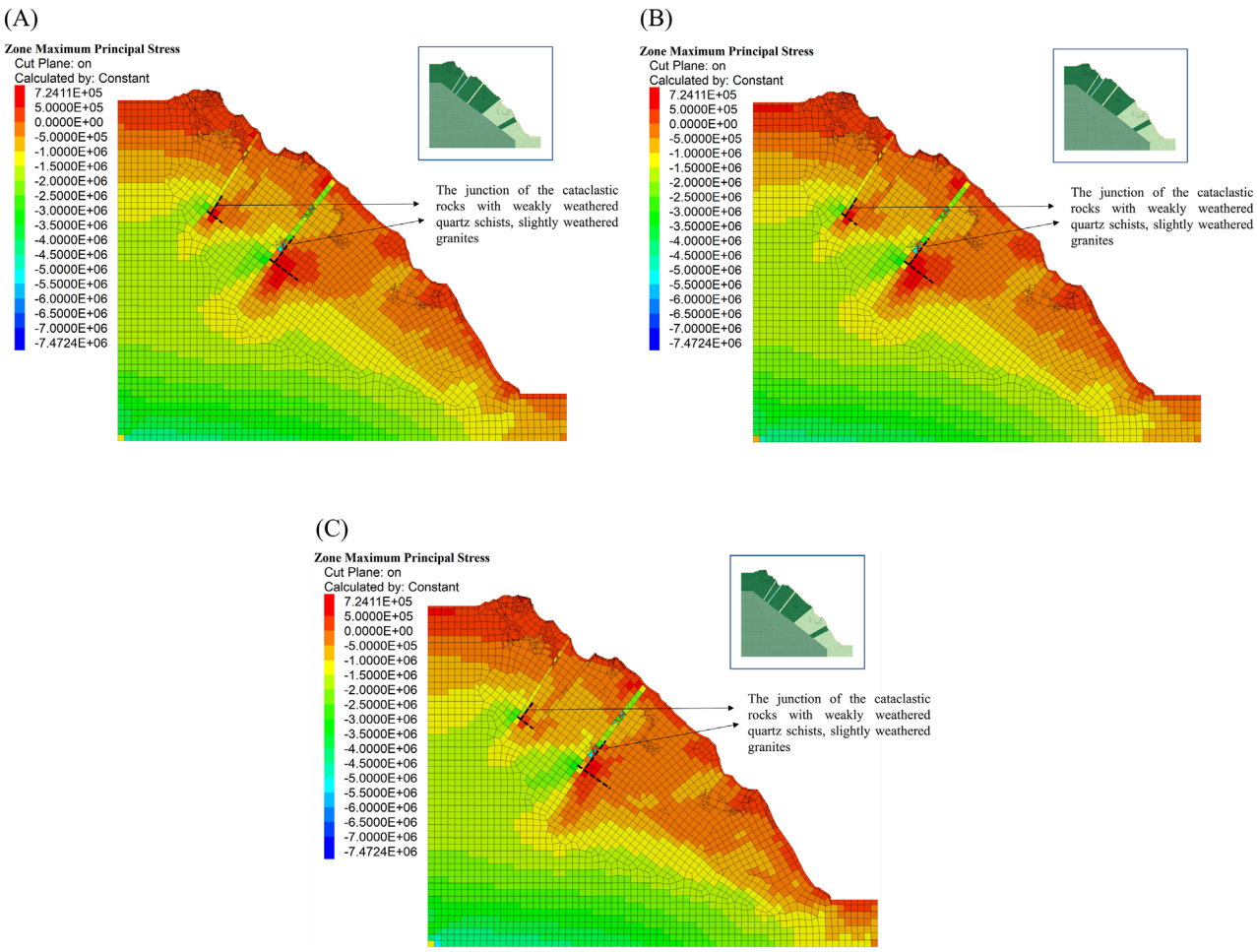

FIGURE 6
The contour of maximum principal stress after the end of seismic and creep action at different amplitudes: **(A)** 0.05 g; **(B)** 0.1 g; **(C)** 0.3 g (unit: Pa).

slope; (2) The initial displacement is cleared to zero, and the Mohr-Coulomb model is assigned to simulate the natural condition; (3) The Mohr-Coulomb model is assigned to all rocks, and the dynamic calculation is carried out by applying bidirectional ground motion at the bottom of the slope; (4) In the creep calculation, the Burgers-Mohr model is applied to the fragmented and strongly weathered quartz schist. The Mohr-Coulomb model is applied to other rocks.

4 Results and discussions

4.1 Analysis of long-term creep response of slope before earthquake

4.1.1 Stress field

As shown in Figure 5A, outside of the cataclastic rock and its influence range, the overall compressive area of the slope accounts for a relatively large proportion of the slope and it shows a more obvious layering phenomenon. Due to the self-weight stress, the compressive stress increases with the slope height decreasing. The compressive stress is about 0–7.63 MPa. The maximum principal stress is 7.63 MPa. It occurs in the middle of the cataclastic rock belt near the middle of the slope because of the small grid division and the element distortion. Its impact can be ignored. Tensile stress mainly appears at the junction of cataclastic rocks with weakly weathered quartz schists and slightly weathered granites, as well as fractured rock mainly at the slope surface of the side slope. The tensile stress is about 0–0.719 MPa.

4.1.2 Displacement field

As shown in Figure 5B, creep occurs mainly in the cataclastic rock distribution region. The maximum displacement reaches 15.39 mm. The maximum creep area is located in the cataclastic rock zone near the middle of the slope. Compared with other rocks, cataclastic rocks have lower compressive strength and more fragmentation, and their discontinuities and fissures are more widely distributed. Therefore, more significant creep deformation will occur in cataclastic rocks. Combined with Figure 5A, the maximum displacement appears in the area of a large distribution of cataclastic rocks which are more broken and looser. The stress is smaller. So the maximum principal stress value is relatively small.

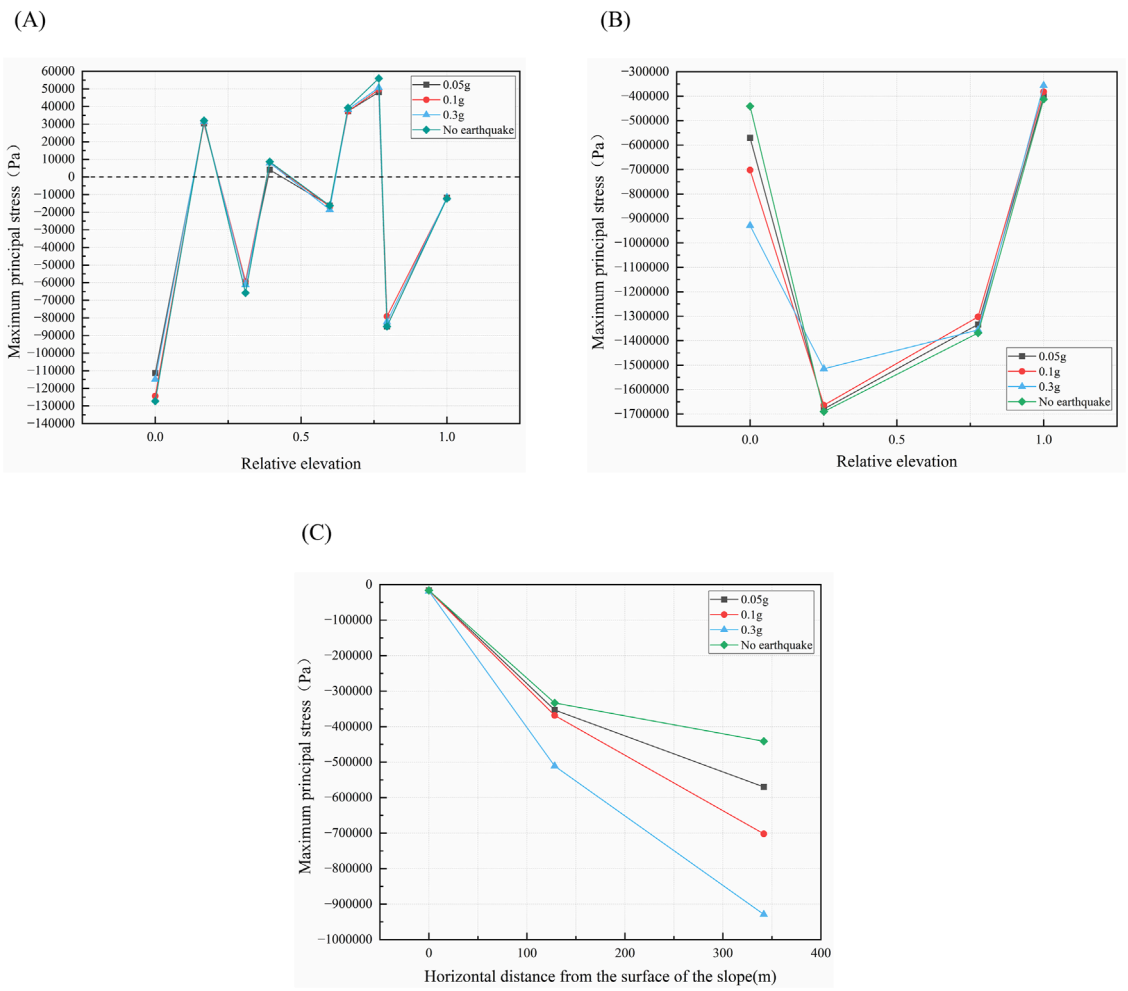

FIGURE 7
Maximum principal stress at each monitoring point in the vertical and horizontal directions: **(A)** Monitoring points on the slope surface; **(B)** Vertical monitoring points in the slope; **(C)** Horizontal monitoring points in the slope.

4.2 Analysis of long-term creep response of slope under seismic action

4.2.1 Stress field

In Figure 6, the stress field shows obvious stress concentration in the localization of the slope, especially at the foot of the slope, the top of the slope, and the demarcation line of the rock structure (unloading zone). Geotectonic activities, crustal changes, and other geologic changes may cause stress accumulation in specific areas, forming areas of high-stress concentration.

Due to the influence of rock structure, lithology, and slope morphology, the maximum principal stress distribution of the slope shows the phenomenon of tensile and compressive stress conversion, which is specifically found at the junction of cataclastic rocks with weakly weathered quartz schists, slightly weathered granites, and in the local area of the fracture zone. The difference of deformation characteristics and the limit of deformed continuous static equilibrium conditions lead to the transformation of tension and compression stress at the interface of three kinds of rocks. A smaller range of tensile stress is distributed in the area of cataclastic rocks, mainly in the middle of the slope surface, where the slope morphology protrudes outwards. That indicates that cataclastic rocks with strong unloading and relaxation may potentially undergo destructive deformations if further impacts are caused by external unfavorable factors. Large tensile stress appears at the shoulder of the slope. Because under the earthquake action, the acceleration near the top of the slope increases rapidly, resulting in instantaneous tensile load which may cause tearing. At three different amplitudes, the overall compressed area of the slope is larger, and the stress contour shows a more pronounced stratification phenomenon. Under the influence of self-weight stress, the maximum principal stress of the slope gradually increases from top to bottom. Excluding the influence of unit distortion, the maximum compressive stress appears at the bottom of the bedrock.

Comparing the maximum principal stress under natural and seismic conditions (Figures 5A, 6), the maximum principal stress is 7.41 Mpa at amplitude 0.05 g, 7.13 Mpa at amplitude 0.1 g and 6.28 Mpa at amplitude 0.3 g.When the amplitude increases, the overall maximum principal stress shows a decreasing trend. The seismic action causes the rock structure to become looser and more

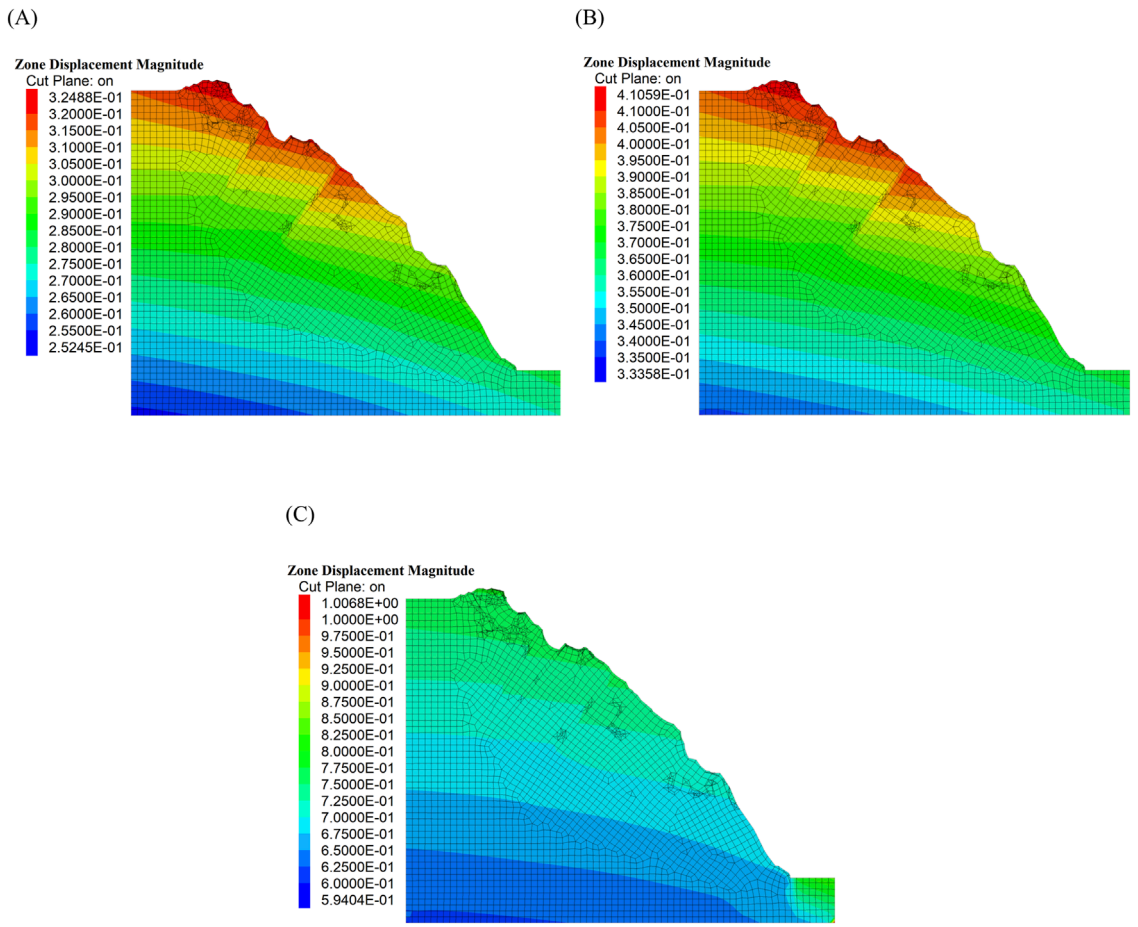

FIGURE 8
The contour of total displacement after the end of seismic and creep action at different amplitudes: **(A)** 0.05 g; **(B)** 0.1 g; **(C)** 0.3 g (unit: Pa).

fragmented, resulting in reduced stress. In particular, the maximum stress value is reduced by 12.6% compared with the natural working condition at amplitude 0.3 g. The slope shear strength decreases and the risk of slope instability increases.

The maximum principal stress at the end of the entire seismic and creep cycle is chosen as the analytical index for Figure 7. This relative elevation is defined as the ratio of the actual slope height h to the total slope height H.

From Figure 7A, at three amplitudes, the curves of maximum principal stress with relative elevation for the slope surface have the same pattern. However, the difference in stress values is not significant, indicating that the amplitude change has a small effect on the maximum principal stress distribution on the slope surface. The maximum compressive stress all occurs at the foot of the slope and the maximum tensile stress all occurs in the middle of the slope. If there are further negative external factors affecting it, the greater tensile stress may pull the upper rock mass and push the lower rock mass to move.

From Figure 7B, at three amplitudes, the trend of the variation of the maximum principal stress with elevation at the vertical monitoring points in the slope is consistent, all of which are compressive stress, showing an increasing and then decreasing trend. Due to the proximity of monitoring points p3 and p4 to the open face, there is a process of stress release, resulting in a rapid decrease in stress.

From Figure 7C, at three amplitudes, the variation trend of the maximum principal stress at the horizontal monitoring points in the slope with respect to elevation is similar, and all are compressive stress. As the amplitude increases, the rate of stress change becomes larger and the maximum principal stress is ranked as follows: 0.3 g > 0.1 g > 0.05 g> natural working condition. The maximum principal stress decreases more rapidly as the slope surface is approached. It reaches a minimum value at the slope surface because stress releases near the critical surface. The presence of tensile and compressive stress at the monitoring points on the slope face and compressive stress at monitoring points inside the slope indicates that the slope face is more unstable compared to the interior of the slope. The maximum principal stresses under the natural working condition are generally greater than those under seismic conditions.

4.2.2 Displacement field

Through Figures 5B, 8, it can be seen that there is a significant difference in the displacement contour of the slope under natural and seismic conditions. This phenomenon may be related to the propagation characteristics of seismic waves, rock material properties, and terrain features. During the earthquake process,

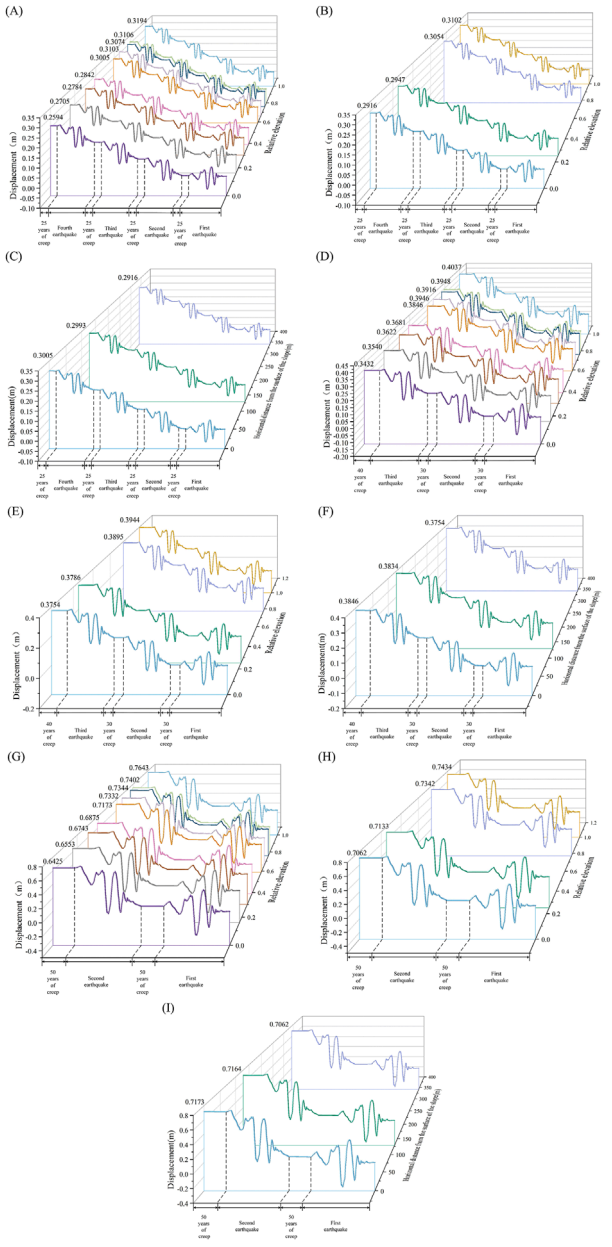

FIGURE 9
Displacement of vertical and horizontal directions for each monitoring point: **(A)** Monitoring points on the slope surface at amplitude 0.05 g; **(B)** Vertical monitoring points in the slope at amplitude 0.05 g; **(C)** Horizontal monitoring points in the slope at amplitude 0.05 g; **(D)** Monitoring points on the slope surface at amplitude 0.1 g; **(E)** Vertical monitoring points in the slope at amplitude 0.1 g; **(F)** Horizontal monitoring points in the slope at amplitude 0.1 g; **(G)** Monitoring points on the slope surface at amplitude 0.3 g; **(H)** Vertical monitoring points in the slope at amplitude 0.3 g; **(I)** Horizontal monitoring points in the slope at amplitude 0.3 g.

seismic waves propagate from bottom to top, causing the redistribution of internal stress and displacement in the slope. The initial stage of displacement shows significant fluctuations and gradually increases. As the seismic activity proceeds, the displacement changes gradually slow down and slowly reach a steady state, forming a permanent displacement. The permanent displacement still exists after the earthquake ends and shows significant differences from the displacement field under the non-earthquake condition. Characteristics of slope materials, such as the shear modulus and the damping ratio, will change. Terrain features may cause amplification effects of seismic waves, which will also affect the distribution of the displacement field.

Through Figures 5B, 8, with the increase of the amplitude, the overall displacement of the slope shows an increasing trend: amplitude 0.3 g > amplitude 0.1 g > amplitude 0.05 g > natural working condition. The overall displacement of the slope is positive and the direction is the positive direction of X-axis. At three amplitudes, the distribution of permanent displacement is in a step-like pattern, mainly distributed on the shoulder, top, and shallow part of the slope, while the displacement response in the middle and lower part of the slope is relatively small. The maximum displacement occurs at the top of the slope, indicating that earthquakes have the greatest impact on the upper-middle part, which is often the starting point for cumulative earthquake damage and crack development. After multiple earthquakes, the slope has experienced accumulated damage on the surface and inside the slope. If there are further adverse external factors in the future, it may lead to large-scale landslides and destruction.

As shown in Figure 9, with the continuous effects of earthquakes and creep, the displacement of the slope shows a continuously increasing trend, exhibiting a certain rhythm. With the increase of amplitudes of seismic waves, the influence of seismic waves gradually increases, and the deformation increases. Each monitoring point displacement is positive which indicates that the slope as a whole is moving outward.

Comparing Figure 9A with Figure 9D, at the amplitude of 0.05 g and 0.1 g, along the vertical direction of the slope, with the increase of height, the displacement first increases, decreases slightly at monitoring point p8 and then increases again, reaching the maximum value at the top of the slope. From Figure 9G, at the amplitude of 0.3 g, the displacement continues to increase with the increase of height and reaches its maximum value at the top of the slope. Regardless of the amplitude, the slope displacement exhibits a significant elevation effect. Combining with Figure 7A, the maximum principal stress value at the top of the slope is smallest and the shear strength is lower which lead to the maximum displacement at the top of the slope.

From Figures 9B, E, H, at three amplitudes, the displacement of cataclastic rocks shows an increasing trend with the increase of elevations. Regardless of whether it is the monitoring point inside the slope or on the slope surface, there is a clear elevation effect. Combining with Figure 7B, the displacement value is maximum at the point where the elevation is maximum. The monitoring point is close to the edge of the slope, where the stress release effect is more significant. Therefore, the corresponding maximum principal stress is the smallest.

From Figures 9C, F, I, at three amplitudes, as the horizontal distance from the slope surface decreases, displacement gradually increases. The displacement value at the monitoring point on the slope's free face reaches its maximum, exhibiting a clear trend towards the slope. Combining with Figure 7C, the displacement near the free face of the slope reaches the maximum. Because there is a stress relief effect at the critical surface. It is consistent with

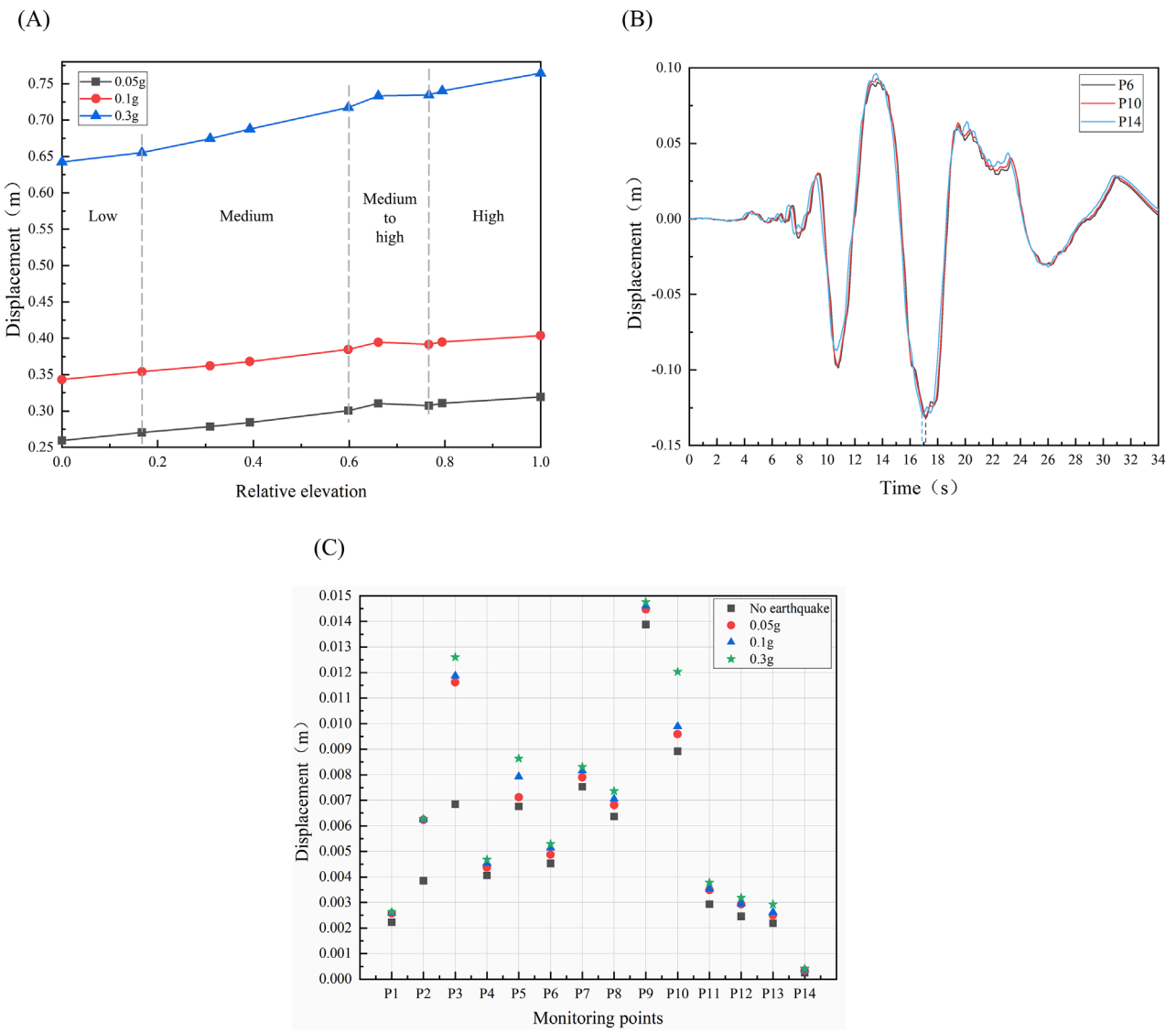

FIGURE 10
Displacement. **(A)** Displacement of each monitoring point on the slope surface after the end of seismic and creep action at different amplitudes. **(B)** Displacement time course curves of three monitoring points on the slope surface during the first seismic stage at amplitude 0.1 g. **(C)** Comparison of 100-year creep displacement under the natural work conditions and earthquakes of different amplitudes.

the pattern of vertical monitoring points on the slope surface and inside the slope.

From Figure 10A, by observing the slope of the displacement change curve, it can be concluded that in the region of relative elevation 0–0.16, the displacement change is not significant; in the region of relative elevation 0.16–0.59, the displacement in the middle of the slope increases rapidly; in the region of relative elevation 0.59–0.76, the increase of the displacement slows down; in the region of relative elevation 0.76–1, the rate of the increase of the displacement increases. It suggests that the earthquake has a greater impact on the central and the top region of the slope. The rate of increase of the folded line corresponding to the amplitude of 0.3 is faster and the curves corresponding to the other two amplitudes have relatively slower increases. Therefore, when the magnitude is larger, the seismic effect on the slope is more significant.

From Figure 10B, as the seismic wave is transmitted, the displacement of each node will oscillate. The displacement waveforms of three monitoring points are consistent and the peak displacement appears close to each other. The moment of peak displacement in the horizontal direction is very close to the moment of peak acceleration of the input horizontal seismic wave. The monitoring point at the top of the slope (p6) shows a slightly delayed time of the peak displacement compared to the peak displacement at the foot of the slope. The process of seismic wave propagation exhibits a delayed effect due to the inertia. The greater the height of the slope is, the more pronounced the delayed effect becomes, and we need to consider the deformation differences of the slope more.

To investigate the effect of seismic actions on creep, the comparison of 100-year creep displacement under the natural working condition and earthquakes of different amplitudes is

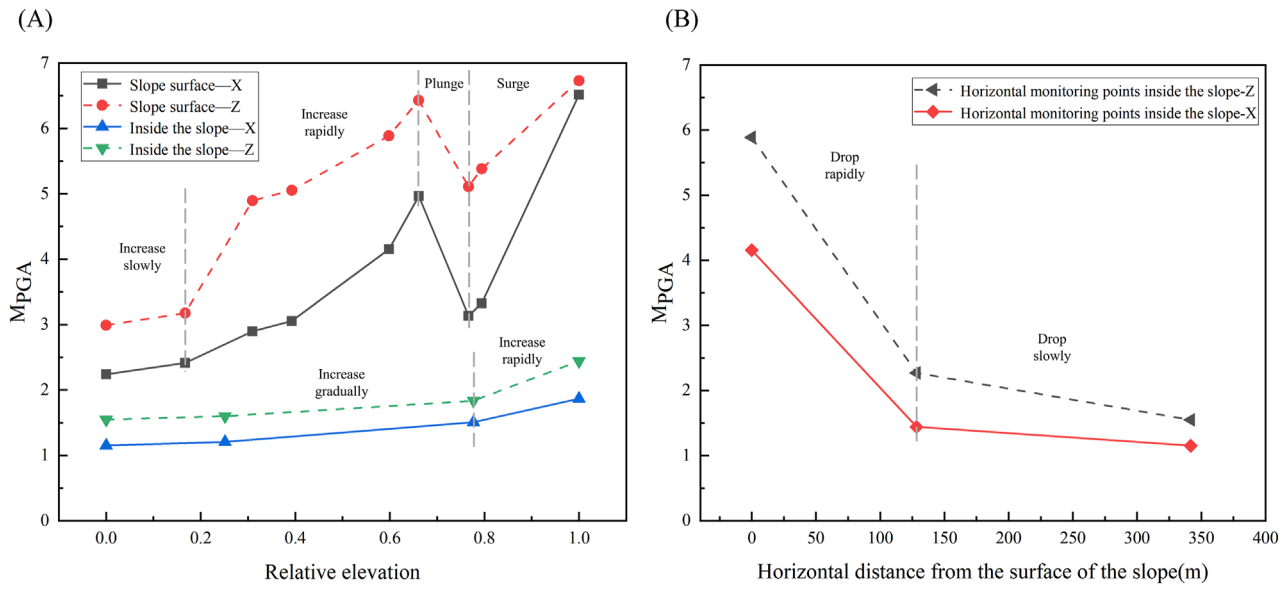

FIGURE 11
M_{PGA} for monitoring points in the vertical and horizontal directions at amplitude 0.1 g: **(A)** Vertical monitoring points on the surface and in the slope along X and Z directions; **(B)** Horizontal monitoring points in the slope along X and Z directions.

conducted (Figure 10C). The 100-year creep displacement ranks as follows: amplitude 0.3 g > Amplitude 0.1 g > amplitude 0.05 g > natural working condition. It shows that the earthquake will promote the development of creep. With the increase of the amplitude, creep displacement shows an increasing trend. For the monitoring points on the slope surface, the creep displacement in the middle of the slope is larger than that in the top and bottom of the slope. For the monitoring points in the slope, the creep displacement of the middle and upper region is larger than that of other regions. This indicates that the earthquake had the greatest impact on the middle of the slope surface, which is consistent with the pattern throughout the end of the seismic and creep cycle.

4.2.3 Dynamic response of acceleration

In order to describe the acceleration response law of the slope, the PGA amplification factors (In the following text, it is referred to as M_{PGA}) is chosen as the analyzing index which is defined as the ratio of the peak acceleration response of each monitoring point to the peak acceleration of the input seismic wave (Antwi Buah et al., 2023). When the amplitude is 0.1 g, the M_{PGA} for monitoring points in the vertical and horizontal directions is shown in Figure 11.

From Figure 11A, the M_{PGA} shows obvious amplification with increasing relative elevation in the vertical direction of the slope, and the amplification shows nonlinearity and segmentation at different elevations. When the slope height is less than 1/5, the M_{PGA} increases slowly at first; from 1/5 to 3/5 of the slope height, the M_{PGA} increases dramatically; from 3/5 to 4/5 of the slope height, the M_{PGA} experiences a significant decline. The reason may be the reflection and refraction of the slope and the fractured weak zone, which leads to the energy concentration in this area of the slope; from 4/5 to the top of the slope height, the acceleration is amplified rapidly, reaching a maximum at the top of the slope, where seismic waves are reflected and superimposed many times, making the amplification effect of seismic waves more intense. It is often where the cumulative destruction of earthquakes and the development of fractures begin. The above phenomena show that the acceleration increment in the middle and upper part of the slope is larger and the seismic response is stronger. It can be seen that the influence of earthquakes on the slope is mainly concentrated in the middle and the top of the slope. It is necessary to strengthen these two parts of the slope, which can reduce the acceleration growth rate. In the horizontal direction of the slope, the M_{PGA} also shows the nonlinear elevation amplification effect and the overall trend of the folding line is consistent with the vertical direction. However, when the height of the slope is over 4/5, the M_{PGA} in the horizontal direction increases faster than that in the vertical direction. The effect of earthquake action on the response of horizontal acceleration is more significant here. Observing the vertical monitoring points in the slope, the changes of the M_{PGA} in horizontal and vertical directions are basically the same. With the increase of relative elevation, the M_{PGA} reaches the maximum value near the air face where the response is obviously stronger than that near the monitoring point inside the slope, showing a surface-trend effect.

From Figure 11B, as the slope surface approaches, the M_{PGA} increases continuously, the amplification rate becomes larger, and the amplification effect of seismic waves becomes stronger. It shows an obvious tendency to the surface.

Both on the slope surface and in the slope, the M_{PGA} of the vertical direction is obviously larger than that of the horizontal direction, which is basically consistent with other scholars' research results (Davis and West, 1973; Cui et al., 2011). The self-oscillation frequency of the slope is similar to the superior frequency of the vertical input seismic wave. The resonance phenomenon of the slope is triggered, resulting in the acceleration amplification effect in the horizontal direction being smaller than that in the vertical direction.

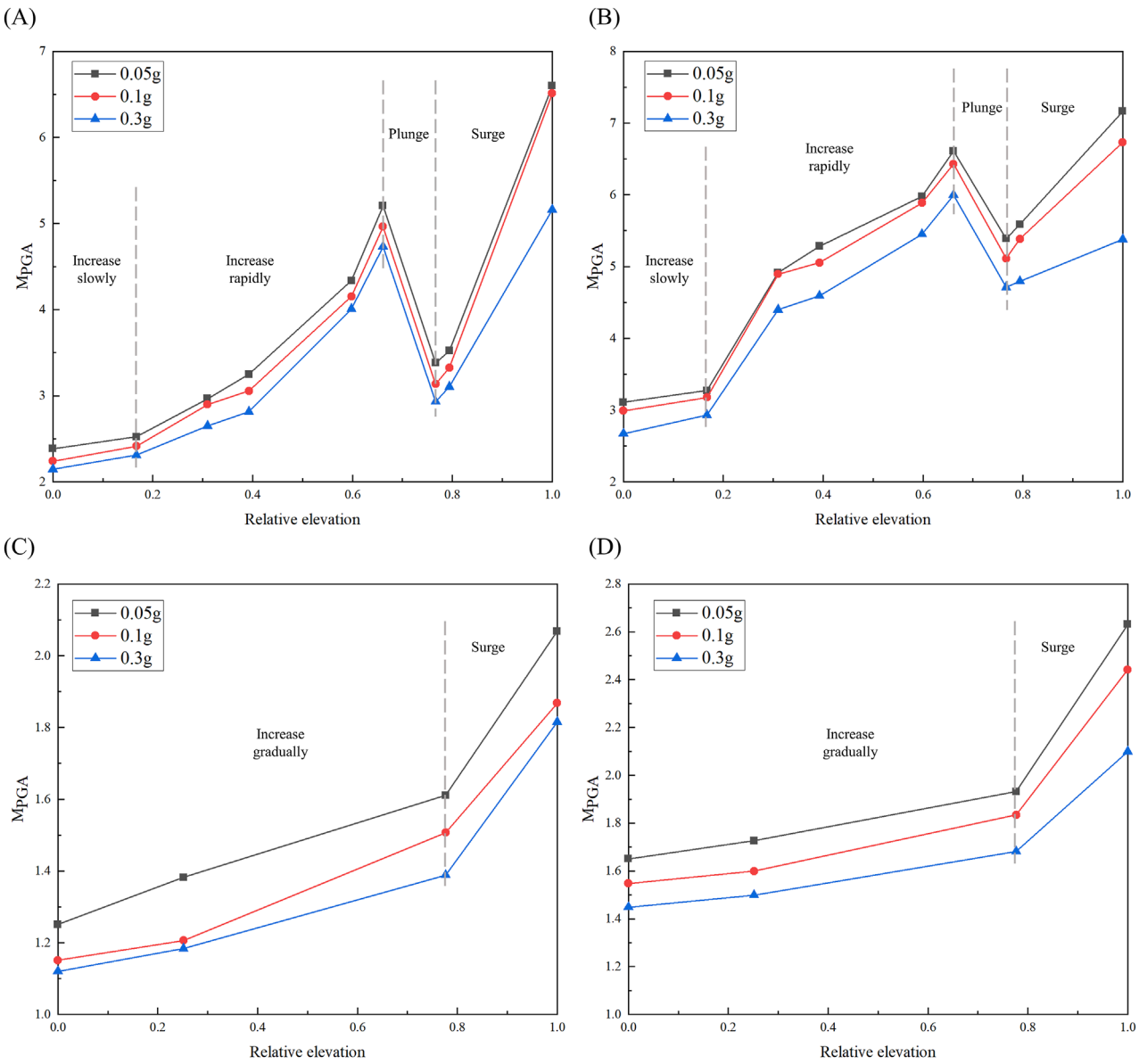

FIGURE 12
The acceleration response of monitoring points on the slope surface and vertical monitoring points in the slope at different amplitudes: **(A)** monitoring points on the slope surface along X direction; **(B)** monitoring points on the slope surface along Z direction; **(C)** vertical monitoring points in the slope along X direction; **(D)** vertical monitoring points in the slope along Z direction.

In order to study the influence of amplitudes on the dynamic response of slope, the results of different amplitudes are compared (Figure 12).

The M_{PGA} decreases with the increase of amplitudes. This rule is consistent with the findings of many scholars (Xu et al., 2008; Yang B. et al., 2018; Xu et al., 2023). The occurrence of this phenomenon may be closely related to the nonlinear properties of the slope rocks, the damping properties, and the frequency of seismic waves. As the intensity of the seismic wave increases, the nonlinear characteristics of rocks become more obvious and its filtering effect is enhanced. At the same time, the strain increases, resulting in a decrease in the shear strength and shear modulus of rocks, an increase in the damping ratio, a decrease in the self-oscillation frequency of the structure and a decrease in the ability to resist deformation. These changes weaken the dynamic response of the slope and reduce the M_{PGA}.

From Figures 12A, B, at different amplitudes, the change rule of the M_{PGA} on the slope surface is basically the same. This indicates that the amplitude has little effect on the acceleration response of the slope surface.

From Figures 12C, D, the M_{PGA} increases continuously with elevation in the horizontal and vertical directions. The closer to the slope surface, the stronger the acceleration amplification effect. When the elevation is less than 4/5, the growth rate is

slow; when the elevation is more than 4/5, the growth rate increases rapidly.

5 Conclusion

In this paper, the finite difference software FLAC3D is used to simulate the process of earthquake action at different amplitudes during 100 years creep. The long-term creep response characteristics of the high rock slope under the cumulative effect of earthquakes are revealed. The main conclusions are as follows:

(1) The combined actions of creep and earthquake increase the risk of slope instability. The increase in amplitudes leads to a looser and more broken rock structure and the overall stress value shows a decreasing trend. Especially, the maximum principal stress is reduced by 12.6% relative to the natural working condition. The shear strength is reduced and the risk of slope instability exists. Tensile and compressive stress are observed at the monitoring points on the slope surface, and all monitoring points in the slope are under compressive stress, making the slope surface more unstable compared to the interior of the slope. The cataclastic rock areas located on the slope face show a combination of compressive and tensile conditions. In the middle of the slope surface, the slope morphology protrudes out-wards, which indicates that cataclastic rocks with strong unloading and relaxation may potentially undergo destructive deformations if further impacts are caused by external unfavorable factors. Large tensile stress also appears at the shoulder of the slope. Because under the earthquake action, the acceleration near the top of the slope increases rapidly, resulting in instantaneous tensile load which may cause tearing.

(2) With the continuous actions of earthquake and creep, when the amplitude increases, the overall displacement tends to increase, and the change curve is rhythmic, reaching the maximum at the top of the slope. It shows the elevation effect and surface-trend effect. Displacement is distributed in a stepwise manner, mainly in the slope shoulder, the shallow surface part of the slope, and at the top of the slope. Earthquakes and creep effects have the greatest impact on the upper and middle parts of the slope which are often places where cumulative damage and crack development begin. Earthquakes promote the development of creep. As the amplitude increases, the 100-year creep displacement tends to increase, and earthquakes have the greatest effect on the area of the middle of the slope surface. Multiple earthquakes coupled with the effects of creep have resulted in the accumulation of damage on the slope surface and in the slope, which could result in widespread landslides and damage in the future if further adverse external influences occur.

(3) In the process of seismic wave propagation upward, the slope presents a delay effect due to inertia. The bigger the slope height is, the more obvious the delay effect is.

(4) The nonlinear height amplification and wave characteristics are obvious in both horizontal and vertical directions. The acceleration response of seismic waves on the slope surface shows a trend of increasing, decreasing and then increasing with elevations, reaching a peak at the top of the slope. The upper part and the middle part of the slope surface have a larger increment and the seismic response is stronger. The M_{PGA} increases continuously with elevation in the horizontal and vertical directions. The closer to the slope surface, the stronger the acceleration amplification effect. The ground motion response on the slope surface is obviously stronger than that in the slope. Therefore, it is necessary to reinforce the middle and top of the slope surface to reduce the risk of instability. Vertical earthquake has a great effect on the dynamic response of the slope. The self-oscillation frequency of the slope is similar to the superior frequency of the vertical input seismic wave. The resonance phenomenon of the slope is triggered, resulting in the acceleration amplification effect in the horizontal direction being smaller than that in the vertical direction. The M_{PGA} decreases with the increase of amplitudes. The occurrence of this phenomenon may be closely related to the nonlinear and damping characteristics of the rock slope and the frequency of seismic waves.

In this study, it can provide some references for the prevention and control of geologic hazards of similar slopes under the combined effects of both creep and earthquakes in the Nujiang River Basin. However, there are some limitations, the slope is only in the stage of elastic deformation and plastic deformation and does not show the sliding instability state. The destabilizing damage mode of the slope needs to be further explored.

Data availability statement

The raw data supporting the conclusions of this article will be made available by the authors, without undue reservation.

Author contributions

MY: Conceptualization, Data curation, Formal Analysis, Investigation, Methodology, Resources, Software, Supervision, Visualization, Writing–original draft, Writing–review and editing. HD: Conceptualization, Funding acquisition, Methodology, Resources, Supervision, Writing–review and editing.

Funding

The author(s) declare that financial support was received for the research, authorship, and/or publication of this article. This research was supported by the Second Tibetan Plateau Scientific Expedition and Research Program (STEP), Grant No. 2019QZKK0906-02.

Conflict of interest

The authors declare that the research was conducted in the absence of any commercial or financial relationships that could be construed as a potential conflict of interest.

Generative AI statement

The author(s) declare that no Generative AI was used in the creation of this manuscript.

Publisher's note

All claims expressed in this article are solely those of the authors and do not necessarily represent those of their affiliated organizations, or those of the publisher, the editors and the reviewers. Any product that may be evaluated in this article, or claim that may be made by its manufacturer, is not guaranteed or endorsed by the publisher.

Supplementary material

The Supplementary Material for this article can be found online at: https://www.frontiersin.org/articles/10.3389/feart.2024.1517953/full#supplementary-material

References

Antwi Buah, P., Zhang, Y. B., He, J. X., Yu, P. C., Xiang, C. L., Fu, H. Y., et al. (2023). Evaluating the dynamic response and failure process of a rock slope under pulse-like ground motions. *Geomatics, Nat. Hazards Risk* 14 (1). doi:10.1080/19475705.2023.2167613

Bao, C. Y., Zhan, L. T., Xia, Y. J., Huang, Y. L., and Zhao, Z. X. (2022). Development trend and stability analysis of creep landslide with obvious slip zone under rainfall-taking Xinchang Xiashan Basalt slope as an example. *Front. Earth Sci.* 9. doi:10.3389/feart.2021.808086

Bao, M., Chen, Z. H., Nian, G. Q., Zhang, L. F., and Zhu, T. Y. (2024). Study on creep properties of weak layer rock of slope under damage coupling. *Bull. Eng. Geol. Environ.* 83 (5), 154. doi:10.1007/s10064-024-03647-4

Bowa, V. M., Xia, Y. Y., Yan, M. J., and Kabwe, E. (2018). Toppling of the jointed rock slope with counter-tilted weak planes influenced by the response to local earthquakes. *Int. J. Min. Mineral Eng.* 9 (4), 302–320. doi:10.1504/ijmme.2018.097427

Büyük, E., Zor, E., and Karaman, A. (2020). Joint modeling of Rayleigh wave dispersion and H/V spectral ratio using Pareto-basedmultiobjective particle swarm optimization. *Turkish J. Earth Sci.* 29 (4), 684–695. doi:10.3906/yer-2001-15

Cai, C., Yu, C. Q., Tao, K., Hu, X. P., Tian, Y., Zhang, H., et al. (2011). Spatial distribution and focal mechanism solutions of the Wenchuan earthquake series: results and implications. *Earthq. Sci.* 24 (1), 115–125. doi:10.1007/s11589-011-0775-5

Che, A. L., Yang, H. K., Wang, B., and Ge, X. R. (2016). Wave propagations through jointed rock masses and their effects on the stability of slopes. *Eng. Geol.* 201, 45–56. doi:10.1016/j.enggeo.2015.12.018

Chen, X. L., Gao, R. X., Gong, W. H., Li, Y., and Peng, Y. H. (2017a). Time history analysis method for seismic reliability of bedding rock slopes based on newmark-beta method. *China J. Highw. Transp.* 30 (7), 33–40. doi:10.19721/j.cnki.1001-7372.2017.07.005

Chen, X. L., Gong, W. H., Zhong, X. H., Qiu, J. W., and Li, Y. (2017b). Dynamic reliability analysis of bedding rock slopes under horizontal and vertical earthquake actions. *China Civ. Eng. J.* 50 (10), 91–98. doi:10.15951/j.tmgcxb.2017.10.012

China earthquake disaster prevention center (2015). Seismic ground motionparameters zonation map of China:GB 18306—2015.

China Earthquake Networks Center (2006). National earthquake data center. Available at: https://data.earthquake.cn (Accessed September 28, 2006).

Chu, Z. F., Wu, Z. J., Liu, Q. S., Weng, L., Xu, X. Y., Wu, K., et al. (2024). Viscos-elastic-plastic solution for deep buried tunnels considering tunnel face effect and sequential installation of double linings. *Comput. Geotechnics* 165 (67), 105930–105961. doi:10.1016/j.compgeo.2023.105930

Cui, F. P., Xu, Q., Tan, R. J., and Yin, Y. P. (2011). Numerical simulation of collapsing and sliding response of slope triggered by seismic dynamic action. *J. Tongji Univ. Sci.* 39 (3), 445–450.

Davis, L. L., and West, L. R. (1973). Observed effects of topography on ground motion. *Bull. Seismol. Soc. Am.* 63 (1), 283–298. doi:10.1785/bssa0630010283

Delchiaro, M., Della Seta, M., Martino, S., Nozaem, R., and Moumeni, M. (2023). Tectonic deformation and landscape evolution inducing mass rock creep driven landslides: the Loumar case-study (Zagros Fold and Thrust Belt, Iran). *Tectonophysics* 846, 229655. doi:10.1016/j.tecto.2022.229655

Deng, D. P., Li, L., and Zhao, L. H. (2014). Research on quasi-static method of slope stability analysis during earthquake. *J. Central South Univ. Sci. Technol.* 45 (10), 3578–3588.

Deng, L. Z., Yuan, H. Y., Zhang, M. Z., and Chen, J. G. (2023). Research progress on landslide deformation monitoring and early warning technology. *J. Tsinghua Univ. Sci. Technol.* 63 (6), 849–864. doi:10.16511/j.cnki.qhdxxb.2023.22.002

Dong, J. Y., Yang, J. H., Wu, F. Q., Yang, G. X., and Huang, Z. Q. (2013). Large-scale shaking table test research on acceleration response rules of bedding layered rock slope and its blocking mechanism of river. *Chin. J. Rock Mech. Eng.* 32, 3861–3867.

Dong, J. Y., Zhao, Y. W., Liu, H. D., Zhao, J. C., Zhang, Z. M., Chi, Q. H., et al. (2023). Creep characteristics of a strongly weathered argillaceous sandstone sliding zone and the disaster evolution mechanism of the Huaipa landslide, China. *Appl. Sciences-Basel* 13 (15), 8579. doi:10.3390/app13158579

Fan, C., Wang, C. H., and Liu, H. B. (2020). Influences of the combined horizontal and vertical excitations on the seismic responses of tiered geosynthetic reinforced slope. *J. Disaster Prev. Mitig. Eng.* 40 (4), 606–613. doi:10.13409/j.cnki.jdpme.2020.04.015

Guo, X. X., Wang, B., Wang, Z. Y., and Yu, J. W. (2023). Methods and practices for deformation prediction in high-stress soft rock tunnels considering creep characteristics. *Chin. J. Geotechnical Eng.* 45 (3), 652–660.

Hu, X. P., Cui, X. F., Ning, J. Y., and Chen, L. W. (2012). Preliminary study on tectonic deformation models in the Longmenshan region based on focal mechanism solutions of the Wenchuan earthquake sequence. *Chin. J. Geophysics-Chinese* 55 (8), 2561–2574. doi:10.6038/j.issn.0001-5733.2012.08.008

Hu, Y. N., Ji, J., Sun, Z. B., and Dias, D. (2023). First order reliability-based design optimization of 3D pile-reinforced slopes with Pareto optimality. *Comput. Geotechnics* 162, 105635. doi:10.1016/j.compgeo.2023.105635

Hu, Y. N., Sun, Z. B., and Ji, J. (2024). Pseudo-dynamic stability analysis of 3D rock slopes considering tensile strength-modified Hoek–Brown failure criterion: seismic UBLA implementations. *Eng. Geol.* 343, 107786. doi:10.1016/j.enggeo.2024.107786

Huang, C., Wang, A. M., and Ren, W. Z. (2010). Influence of time combination pattern of horizontal and vertical ground motions on slope seismic safety factor. *Rock Soil Mech.* 31 (11), 3404–3410. doi:10.16285/j.rsm.2010.11.005

Huang, W. P., Sun, Y. X., and Chen, S. J. (2021). Theory of creep disturbance effect of rock and its application in support of deep dynamic engineering. *Chin. J. Geotechnical Eng.* 43 (9), 1621–1630. doi:10.11779/CJGE202109006

Huang, Z. Q., Li, J. L., Wang, C., Cao, S. C., and Yuan, G. X. (2023). Study on dynamic response and failure mode of steep bedding rock slope under strong earthquake. *J. Eng. Geol.* 31 (1), 217–227. doi:10.13544/j.cnki.jeg.2020-544

Institute of Geophysics, C. E. A. (2004). China earthquake Networks center. Available at: https://news.ceic.ac.cn/index.html?time=1727524519 (Accessed October, 18).

Itasca Consulting Group (2020). FLAC3D 7.0 modelling. Available at: https://docs.itascacg.com/flac3d700/flac3d/docproject/source/flac3dhome.html.

Jeng, C. J., Chen, S. S., and Tseng, C. H. (2022). A case study on the slope displacement criterion at the critical accelerated stage triggered by rainfall and long-term creep behavior. *Nat. Hazards* 112 (3), 2277–2312. doi:10.1007/s11069-022-05265-3

Ji, J., Lin, Z. J., Li, S. K., Song, J., and Du, S. G. (2024). Coupled Newmark seismic displacement analysis of cohesive soil slopes considering nonlinear soil dynamics and post-slip geometry changes. *Comput. Geotechnics* 174, 106628. doi:10.1016/j.compgeo.2024.106628

Jiang, S., Wen, B. P., Jiang, X. Z., Li, R. D., and Zhao, C. (2019). A non-linear damage rheological constitutive model and its application to a giant slow-moving landslide. *Hydrogeology and Eng. Geol.* 46 (1), 56–63. doi:10.16030/j.cnki.issn.1000-3665.2019.01.08

Lei, Q. H., and Sornette, D. (2023). A stochastic dynamical model of slope creep and failure. *Geophys. Res. Lett.* 50 (11). doi:10.1029/2022gl102587

Li, A. R., Deng, H., Zhang, H. J., Jiang, M. L., Liu, H. H., Xiao, Y. Y., et al. (2021a). Developing a two-step improved damage creep constitutive model based on soft rock saturation-loss cycle triaxial creep test. *Nat. Hazards* 108 (2), 2265–2281. doi:10.1007/s11069-021-04779-6

Li, M. J., Qiao, L., Tian, Y., and Du, H. R. (2021b). Analysis of deformation mechanism of soft rock composite slope in open-pit mine. *Coal Sci. Technol.* 49 (8), 108–113. doi:10.13199/j.cnki.cst.2021.08.014

Li, R. J., Ji, F., Feng, W. K., Wang, D. P., and Zhang, J. M. (2019). Shear creep characteristics and constitutive model of hidden non-persistent joints. *Chin. J. Geotechnical Eng.* 41 (12), 2253–2261. doi:10.11779/CJGE201912010

Li, X. W. (2015). *The analysis of the stability of bedding slope under the effect of frequent seismic*. Master Thesis: Chongqing University.

Lian, J., Ding, X. M., and Zhang, L. (2023). Shaking table test on seismic response of an accumulation landslide reinforced by pile-plate retaining wall based on the time-frequency analysis method. *J. Central South Univ.* 30 (5), 1710–1721. doi:10.1007/s11771-023-5323-7

Liu, X. R., He, C. M., Liu, S. L., Liu, Y. Q., Lu, Y. M., and Liu, Z. H. (2018). Dynamic response and failure mode of slopes with horizontal soft and hard interbeddings under frequent microseisms. *Arabian J. Sci. Eng.* 43 (10), 5397–5411. doi:10.1007/s13369-018-3143-0

Luo, Y., Li, J., and Hu, B. (Year) (2008). "Flowing deformation of softrock and deformation and wreck of slope," in *The 8th national conference on engineering geology* (Shanghai, China), 226–229.

Lysmer, J., and Kuhlemeyer, R. L. (1969). Finite dynamic model for infinite media. *J. Eng. Mech. Div.* 95 (4), 859–877. doi:10.1061/jmcea3.0001144

Ministry of Construction of the People's Republic of China (2009). *Code for seismic design of railway engineering:GB 50111-2006*. 2009 edition.

Paul, K., Bhattacharya, P., and Misra, S. (2024). Frictional control on accelerating creep during the slow-to-fast transition of rainfall-induced catastrophic landslides. *J. Geophys. Research-Earth Surf.* 129 (1). doi:10.1029/2023jf007213

Peng, Y. H. (2017). *Research on stability of bedding rock slope under bidirectional earthquake*. Master Thesis: Huazhong University of Science and Technology.

Seismosoft (2021). Seismosignal software. Available at: https://seismosoft.com/(Accessed December 21, 2021).

Song, D. Q., Che, A. L., Zhu, R. J., and Ge, X. R. (2018). Dynamic response characteristics of a rock slope with discontinuous joints under the combined action of earthquakes and rapid water drawdown. *Landslides* 15 (6), 1109–1125. doi:10.1007/s10346-017-0932-6

Song, G. F., Du, J. M., Ke, J., Deng, Q., and Liang, Y. F. (2019). Stability limit analysis of bedding rock slopes based on pseudo-dynamic method. *China Earthq. Eng. J.* 41 (4), 931–938.

Sun, C., Jin, C. Z., Wang, L. G., Cai, J. Q., and Li, J. D. (2023). Creep damage characteristics and slip law of weak-layer mudstone in an open mining slope. *Bull. Eng. Geol. Environ.* 82 (10), 399. doi:10.1007/s10064-023-03414-x

Sun, H., Wu, H. G., Ma, Z. G., Yuan, Z., and Feng, K. (2022). Analysis of seismic damage modes of landslides containing tunnels under horizontal earthquake action. *Geofluids* 2022, 1–18. doi:10.1155/2022/6026316

Sun, Z. L., Kong, L. W., and Guo, A. G. (2017). Dynamic centrifuge tests on seismic responses of air-dried deposit slopes. *Chin. J. Rock Mech. Eng.* 36 (9), 2102–2112. doi:10.13722/j.cnki.jrme.2017.0077

Tang, H., Wu, Z. J., Che, A. L., Yuan, C. H., and Deng, Q. (2021). Failure mechanism of rock slopes under different seismic excitation. *Adv. Mater. Sci. Eng.* 2021. doi:10.1155/2021/8866119

Vallet, A., Charlier, J. B., Fabbri, O., Bertrand, C., Carry, N., and Mudry, J. (2016). Functioning and precipitation-displacement modelling of rainfall-induced deep-seated landslides subject to creep deformation. *Landslides* 13 (4), 653–670. doi:10.1007/s10346-015-0592-3

Wang, X., Liu, H., and Song, E. (2011). Effect of earthquake type on dynamic response of geosynthetic-reinforced soil walls after long-term creep. *J. Hohai Univ. Nat. Sci.* 39 (5), 528–535.

Wen, Y. M., Xu, C. J., Li, Z. H., Liu, Y., Feng, W. P., and Shan, X. J. (2014). Coseismic and postseismic deformation of the 2008 wenchuan earthquake from InSAR. *Chin. J. Geophysics-Chinese* 57 (6), 1814–1824. doi:10.6038/cjg20140613

Xiong, S., Li, D. Q., Liu, Y., and Du, W. Q. (2023). Effect of weak intercalated layers on the seismic response of rock slopes based on numerical analysis. *J. Earthq. Eng.* 27 (16), 4595–4612. doi:10.1080/13632469.2023.2185865

Xu, G. X., Yao, L. K., Gao, Z. N., and Li, Z. H. (2008). Large-scale shaking table model test study on dynamic characteristics and dynamic responses of slope. *Chin. J. Rock Mech. Eng.* 27 (3), 624–632.

Xu, M., Yu, X. Y., Zhao, Y. P., Hu, J. J., and Zhang, X. T. (2023). Analysis of seismic dynamic response and failure mode of bedding rock slope with laminated fractured structure. *Rock Soil Mech.* 44 (2), 362–372. doi:10.16285/j.rsm.2022.0438

Xu, N. W., Li, T., Dai, F., Li, B., Fan, Y. L., and Xu, J. (2017). Stability analysis on the left bank slope of Baihetan hydropower station based on discrete element simulation and microseismic monitoring. *Rock Soil Mech.* 38 (8), 2358–2367. doi:10.16285/j.rsm.2017.08.025

Yan, Z. X., Li, Y. P., Long, Z., and Zhai, J. Y. (2020). Shearing action of anchorage interface of rock slope with soft layer under bidirectional coupled earthquake. *J. Vib. Shock* 39 (11), 158–164. doi:10.13465/j.cnki.jvs.2020.11.021

Yan, Z. X., Zhang, S., Zhang, X. D., and Zhang, L. P. (2011). Study of dynamic response of bedding rock slope under earthquake and influence of ground motion parameters. 30(S2), 3522–3528.

Yang, B., Yang, X., Yang, T., Wang, R., and Zhou, D. (2018a). Shaking table model test on dynamic response and failure process of shatter-burst sliding slope under earthquake load. *Chin. J. Rock Mech. Eng.* 37, 3279–3290. doi:10.13722/j.cnki.jrme.2016.1256

Yang, Z. P., Liu, S. L., Liu, Y. Q., He, C. M., and Yang, W. (2018b). Dynamic stability analysis of bedding and toppling rock slopes under repeated micro-seismic action. *Chin. J. Geotechnical Eng.* 40 (7), 1277–1286.

Yu, Y. (2016). Establishment and characteristic analysis of the attenuation relationship of ground motion parameters in the new generation seismic zoning map. *City Disaster Reduct.* 3, 34–38.

Yuan, H. P., Cao, P., Wan, W., and Xu, W. Z. (2006). Study on creep rules of soft and intricate ore-rock under step load and unload. *Chin. J. Rock Mech. Eng.* 25 (8), 1575–1581.

Zhang, H., Zhao, H. B., Zhang, X. Y., Wang, T., Li, H. H., and Wang, Y. (2019). Creep characteristics and model of key unit rock in slope potential slip surface. *Int. J. Geomechanics* 19 (8). doi:10.1061/(asce)gm.1943-5622.0001486

Zhen, Z. X. (2021). Modified time-varying damage model with caputo fractional derivative on the creep destruction prediction of rock slope. *Math. Problems Eng.* 2021, 1–5. doi:10.1155/2021/6670362

Zhou, J. F., Zheng, Z. y., Bao, T., Tu, B. X., Yu, J., and Qin, C. b. (2023). Assessment of rigorous solutions for pseudo-dynamic slope stability: finite-element limit-analysis modelling. *J. Central South Univ.* 30 (7), 2374–2391. doi:10.1007/s11771-023-5370-0

Zhou, X. P., and Cheng, H. (2015). The long-term stability analysis of 3D creeping slopes using the displacement-based rigorous limit equilibrium method. *Eng. Geol.* 195, 292–300. doi:10.1016/j.enggeo.2015.06.002